Anti-inflammatory and cytotoxic specialised metabolites from the leaves of *Glandularia × hybrida*

Nesma M. Mohamed [a], Mai A.M. Ahmed [a], Shabana I. Khan [b,c], Frank R. Fronczek [d], Anber F. Mohammed [e], Samir A. Ross [b,c,*]

[a] *Department of Pharmacognosy, Faculty of Pharmacy, Assiut University, Assiut, 71526, Egypt*
[b] *National Center for Natural Products Research, Research Institute of Pharmaceutical Sciences, School of Pharmacy, University of Mississippi, University, MS, 38677, USA*
[c] *Division of Pharmacognosy, Department of BioMolecular Sciences, School of Pharmacy, University of Mississippi, University, MS, 38677, USA*
[d] *Department of Chemistry, Louisiana State University, Baton Rouge, LA, 70803, USA*
[e] *Department of Pharmaceutical Organic Chemistry, Faculty of Pharmacy, Assiut University, Assiut, 71526, Egypt*

ARTICLE INFO

ABSTRACT

In our ongoing effort to investigate active specialised metabolites from genus *Glandularia,* phytochemical studies on the ethanolic extract of *Glandularia × hybrida* (Groenl. & Rümpler) G.L. Nesom & Pruski leaves resulted in the isolation of three undescribed compounds, a dibenzylbutyrolactolic lignan and two echinocystic acid based triterpenoid saponins, in addition to two known compounds. Interestingly, this study reports isolation of chemosystematically valuable specialised metabolites for the first time from the genus under investigation. Additionally, the isolated metabolites were evaluated for their iNOS inhibition and cytotoxic activities using a combination of *in silico* and *in vitro* studies. The pharmacokinetics properties (ADMET) of some of the isolated compounds were determined using pkCSM-pharmacokinetics server. Molecular docking analysis showed that saponin compound possesses higher negative score (-9.59 kcal/mol) than the lignan compound (-6.56 kcal/mol). The isolated compounds also showed iNOS inhibition activity with IC_{50} values ranging between 6.6 and 49.7 μM and significant cytotoxic activity against a series of cell lines including SK-MEL, KB, BT-549, SK-OV-3, LLC-PK1 and VERO cells. Hence, this study reveals that specialised metabolites from *G. hybrida* plant are of significant anti-inflammatory and cytotoxicity potentials.

1. Introduction

Glandularia J. F. Gmel. (Verbenaceae) is a genus of about 84 species, mainly distributed in the temperate areas of North and South America (O'Leary and Thode, 2016). It is one of the genera which is phylogenetically linked to the genus *Verbena.* It is considered as a sister genus in the Verbena complex that comprises three genera i.e. *Verbena, Glandularia* and *Junellia* (Yuan and Olmstead, 2008). Recent phytochemical studies on the genus *Glandularia* have reported the identification of saponins, iridoids and flavonoids (Vestena et al., 2019; Mohamed et al., 2020; Ahmed et al., 2021). Unlike *Verbena*, no extensive investigation has been conducted on the phytoconstituents of *Glandularia*. *Glandularia × hybrida* (Groenl. & Rümpler) G. L. Nesom & Pruski was known as *Verbena × hybrida* (Pruski and Nesom, 1992). It is an annual,

floricultural, very charming ornamental plant, and commonly named as Garden Verbena (Mabberley, 2017). Our previous phytochemical and biological studies on *G. hybrida* roots revealed the presence of ursane and oleanane-type triterpenoid saponins with notable anti-inflammatory activity (Mohamed et al., 2020). Thus, we become more interested in these scaffolds and this provoked us to profile the characteristic specialised metabolites of the leaves of *G. hybrida*. Interestingly, this study reports chemo-systematically significant isolation and identification of three undescribed compounds (**1–3**) i.e. a dibenzylbutyrolactolic lignan and two echinocystic acid based triterpenoid saponins, from the ethanolic extract of *G. hybrida* leaves for the first time from this genus. The compounds were evaluated for their *in vitro* cytotoxic activity against human cancer cell lines including SK-MEL, KB, BT-549, SK-OV-3 and LLC-PK1 cells. The anti-inflammatory activity of

---

the isolated compounds was also determined through cellular assay targeting the inhibition potential of the compounds against iNOS inflammatory mediator. Inhibitory activity of isolated compounds against iNOS was evaluated using both *in silico* and *in vitro* studies.

2. Results and discussion

The defatted fraction obtained from the ethanolic extract of *G. hybrida* leaves was subjected to a series of chromatographic techniques to afford five compounds (**1-5**), from which three compounds (**1–3**) are previously undescribed. They were identified as dibenzylbutyrolactolic lignan (**1**) and echinocystic acid based triterpenoidal saponins (**2** and **3**), with their structures elucidated on the basis of 1D, 2D-NMR and HRESIMS. The ^{1}H and ^{13}C-NMR data are shown in Tables 1 and 2, and the spectra are given in the Supporting Information (Figures S1–S24).

2.1. Structural elucidation of isolated compounds

Compound **1** was obtained as a colourless residue, its molecular formula was deduced as $C_{20}H_{20}O_7$ on the basis of molecular ion peaks [M-H]$^-$ at m/z 371.1176 (calcd. for $C_{20}H_{19}O_7$, 371.1131), and [M + HCOO]$^-$ at m/z 417.1219 (calcd. for $C_{21}H_{21}O_9$ 417.1191) in negative mode HRESIMS (Fig. S8). The ^{1}H-NMR spectrum (Fig. S1) (Table 1) showed two singlets at δ_H 5.94 and 5.95 (s, C-10 & 10′) characteristic for two aromatic methylenedioxy groups. A group of signals, six protons appeared between δ_H 6.55 and 6.80, attributable to six aromatic protons characteristic for two moieties of 1,3,4-tri-substituted aromatic rings. In addition, ^{1}H-NMR spectrum (Table 1) displayed signals for a methine group at δ_H 2.39 (m, H-8′), an oxygenated methine at δ_H 4.72 (d, J = 4.0 Hz, H-9), an oxygenated methylene at δ_H 3.53 (t, J = 6.4 Hz, H-9a′) and δ_H 3.70 (t, J = 6.4 Hz, H-9b′), two benzylic protons at δ_H 2.69 (d, J = 10.8 Hz, H-7a) and δ_H 2.79 (d, J = 10.8 Hz, H-7b), as well as another two benzylic protons appear at δ_H 2.37 (m, H-7′). The ^{13}C-NMR spectrum (Fig. S2 and S3) (Table 1), in combination with the HMQC spectrum (Fig. S4), showed signals for twenty carbon atoms, twelve aromatic carbons including six quaternary carbons and six tertiary carbons (δ_C 107.5–147.2), an oxygenated methylene carbon (δ_C 71.1), two di-oxygenated methylene carbons (δ_C 100.4 & 100.6), a di-oxygenated methine carbon (δ_C 102.8), an oxygenated quaternary carbon (δ_C

Table 1
^{1}H and ^{13}C-NMR data of compound **1** (400/100 MHz, δ in ppm, J values in Hz) in DMSO-d_6

Position	δ_C	δ_H
1	132.0	–
2	110.9	6.91 (br s)
3	147.2	–
4	145.2[b]	–
5	107.5	6.78[a]
6	123.5	6.80[a]
7	39.9	2.69 (d, 10.8)
		2.79 (d, 10.8)
8	81.1	–
9	102.8	4.72 (d, 4.0)
1′	134.9	–
2′	108.8	6.73 (d, 1.6)
3′	146.5	–
4′	145.3[b]	–
5′	108.1	6.79[a]
6′	121.1	6.60 (dd, 8.0, 1.6)
7′	31.9	2.37 (m)
8′	45.9	2.39 (m)
9′	71.1	3.53 (t, 6.4)
		3.70 (t, 6.4)
10	100.4[b]	5.94 (s)
10′	100.6[b]	5.95 (s)

[a] Unclear signal pattern due to overlapping.
[b] Values are interchangeable.

Table 2
^{1}H and ^{13}C-NMR data of compounds **2** and **3** (δ in ppm, J values in Hz)

Position	Compounds			
	2[b]		**3**[c]	
	δ_H	δ_C	δ_H	δ_C
1	1.50 (m)	39.4	1.49 (m)	38.3
	0.95 (m)		0.88 (m)	
2	2.26 (m)	27.2	1.83 (m)	25.7
	1.89 (m)		1.50 (m)	
3	3.41 (dd, 9.6, 3.2)	89.4	3.01[a]	88.7
4	–	40.0	–	38.7
5	0.82 (m)	56.4	0.65 (m)	55.6
6	1.50 (m)	19.1	1.44 (m)	17.7
	1.37 (m)		1.22 (m)	
7	1.65 (m)	34.0	1.36 (m)	32.6
	1.46 (m)		1.26 (m)	
8	–	40.5	–	39.8
9	1.78 (m)	47.6	1.50 (t, 9.6)	46.5
10	–	37.5	–	36.4
11	1.96 (m)	24.4	1.79 (m)	22.8
12	5.65 (br s)	123.5	5.22 (br s)	122.0
13	–	144.9	–	143.8
14	–	42.6	–	41.2
15	2.23 (m)	36.6	1.58[a]	34.7
	1.85 (m)		1.23[a]	
16	5.31 (br s)	74.5	4.38 (br s)	72.5
17	–	50.1	–	48.3
18	3.61 (br d, 13.8)	41.8	2.90[a]	40.1
19	1.39 (m)	47.7	0.95 (m)	46.3
	2.81 (m)		2.20 (t, 12.4)	
20	–	31.5	–	30.2
21	2.44 (m)	36.5	1.88 (m)	35.0
	1.32 (m)		1.04 (m)	
22	2.35 (m)	32.7	1.77 (m)	31.1
	2.22 (m)		1.59 (m)	
23	1.31 (s)	28.8	0.93 (s)	27.8
24	1.01 (s)	17.6	0.71 (s)	16.6
25	0.88 (s)	16.3	0.83 (s)	15.7
26	1.12 (s)	18.1	0.61 (s)	17.1
27	1.83 (s)	27.8	1.27 (s)	26.8
28	–	176.5	–	175.2
29	1.04 (s)	33.8	0.81 (s)	33.2
30	1.18 (s)	25.3	0.88 (s)	24.6
3-O-β-D-Glu				
1	4.95 (d, 8.0)	107.4	4.23 (d, 7.6)	104.4
2	4.07 (m)	76.3	3.14 (m)	78.2
3	4.27 (m)	79.2	3.25 (m)	77.4
4	4.15 (m)	71.7	3.03 (m)	70.9
5	4.02 (m)	78.7	3.78[a]	77.1
6	4.43 (m)	62.8	3.70[a]	61.1
	4.58 (m)		3.39[a]	
β-D-Apiose (at C-2 Glu)				
1			5.28 (d, 2.4)	109.4
2			3.80 (d, 2.4)	76.8
3			–	79.3
4			3.86 (d, 7.6)	73.9
			3.52[a]	
5			3.33 (m)	64.1
28-O-α-L-Ara (ester)				
1	6.56 (br s)	93.7	5.52 (br s)	91.9
2	4.55 (m)	76.3	3.56 (m)	76.3
3	4.61 (m)	69.9	3.64[a]	70.2
4	4.47 (m)	66.1	3.63[a]	64.3
5	3.97 (m)	63.5	3.61 (m)	61.4
	4.58 (m)		3.39 (m)	
α-L-Rham-I (at C-2 Ara)				
1	5.66 (br s)	101.9	4.76 (br s)	99.3
2	4.72 (m)	72.3	3.67[a]	70.5
3	4.56 (m)	81.6	3.65[a]	79.1
4	4.54 (m)	77.9	3.52 (m)	76.8
5	4.39 (m)	69.5	3.48[a]	67.7
6	1.73 (d, 6.4)	19.2	1.09 (d, 6.0)	18.1
α-L-Rham-II (at C-3 Rha-I)				
1	5.85 (br s)	105.0	4.81 (br s)	102.7
2	5.07 (br s)	72.8	3.77[a]	70.5
3	4.59 (m)	73.3	3.50 (m)	70.2

Table 2 (*continued*)

Position	Compounds			
	2[b]		3[c]	
	δ_H	δ_C	δ_H	δ_C
4	4.28 (m)	74.6	3.17 (m)	72.8
5	4.60 (m)	70.7	3.63 (m)	68.8
6	1.55 (d, 6.4)	19.1	1.08 (d, 6.0)	18.2
β-D-Xyl (at C-4 Rha-I)				
1	5.18 (d, 7.6)	105.9	4.32 (d, 7.8)	103.8
2	3.95 (m)	75.7	2.88 (m)	74.1
3	4.11 (m)	78.6	3.13 (m)	76.8
4	4.14 (m)	71.6	3.23 (m)	70.2
5	3.37[a]	67.6	3.68[a]	66.0
	4.15 (m)		2.94 (m)	

[a] Unclear signal pattern due to overlapping.
[b] Compound **2** data reported in pyridine-d_5 (400/100 MHz).
[c] Compound **3** data reported in DMSO-d_6 (600/150 MHz).

81.8), three upfield carbons including two methylene carbons (δ_C 31.9 & 39.9) and one methine carbon (δ_C 45.9). The provided data was found to be closely related to the reported data of the bioactive naturally occurring lignan cubebin (**1a**) (Vidigal et al., 1995; Macedo et al., 2020), except for the presence of an additional hydroxyl group. The placement

of this additional hydroxyl group was determined on the basis of $^1H–^1H$ COSY and HMBC experiments. In HMBC spectrum (Fig. S5) (Fig. 2), obvious correlations was found between CH$_2$-7 at δ_H 2.69 and δ_H 2.79 with C-1 (δ_C 132.0), C-2 (δ_C 110.9), C-6 (δ_C 123.5), C-8 (δ_C 81.8), C-9 (δ_C 102.8), between H-8′ at δ_H 2.39 with C-1′ (δ_C 134.9), C-7′ (δ_C 31.9) and C-9′ (δ_C 71.1), and between methylenic protons CH$_2$-9′ at δ_H 3.53 and δ_H 3.70 with C-7′ (δ_C 31.9), C-8 (δ_C 81.8), and C-8′ (δ_C 45.9). Furthermore, the $^1H–^1H$ COSY spectrum (Fig. S6) (Fig. 2) showed correlations between H-7′ (δ_H 2.37), H-8′ (δ_H 2.39) and H-9′ (δ_H 3.53 & 3.70). All the provided correlations recommend the placement of the hydroxyl group at position C-8.

X-ray crystallographic analysis was used to determine unequivocally the configuration of the hydroxyl group on C-8 and confirm the configuration of the asymmetric centres of **1**. A single crystal suitable for X-ray analysis was obtained by recrystallization of **1** from methanol solution. The crystallographic data confirmed the structure and revealed that the additional hydroxyl group attached to C-8, together with all asymmetric centres are of the *S* configuration (Fig. 3). The absolute configuration was determined from the Flack parameter (Parsons et al., 2013) x = 0.14(18) based on 1017 quotients and from the Hooft parameter (Hooft et al., 2008) y = 0.07(15) based on 1406 Bijvoet pairs (99% coverage), corresponding to a probability of 1.000 that the
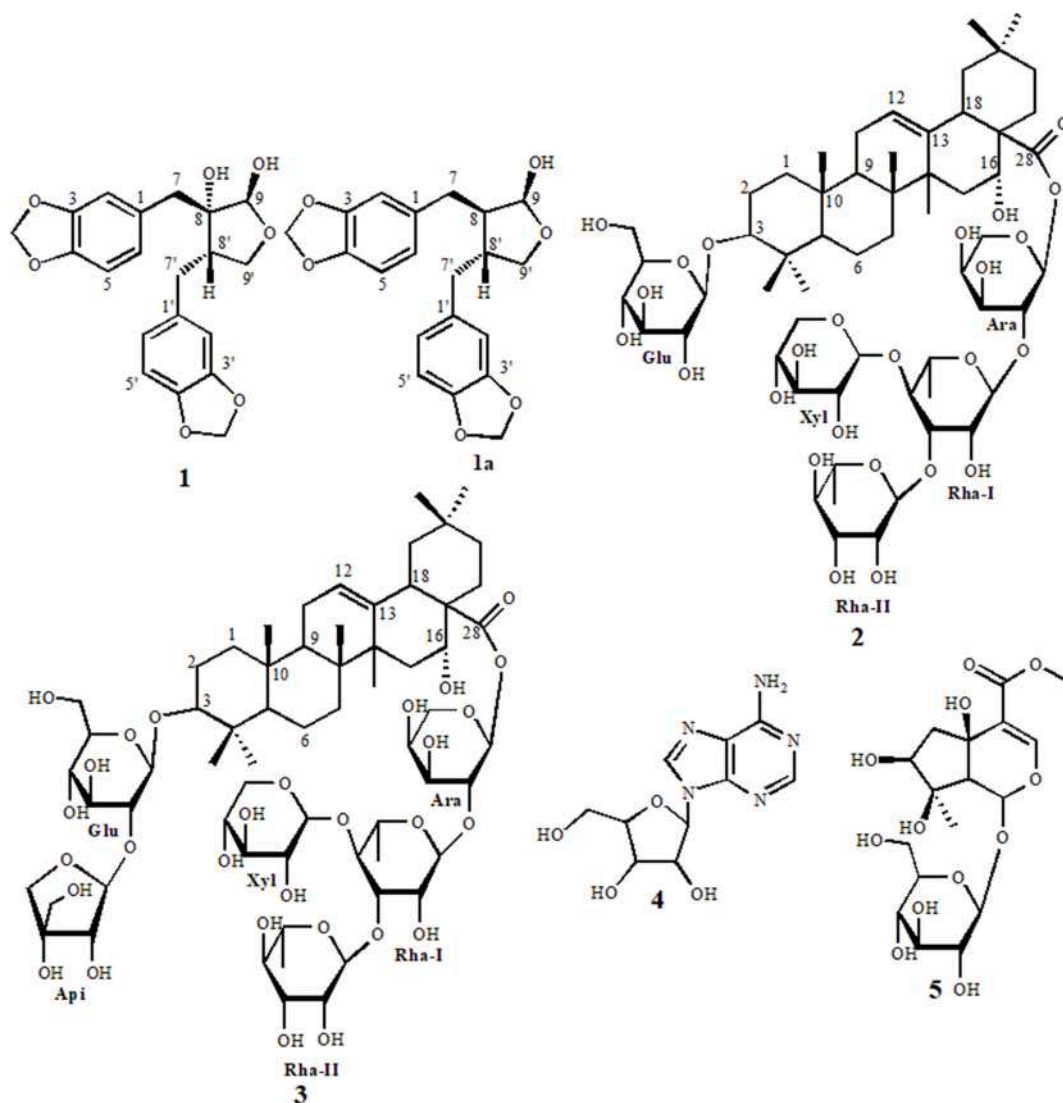

Fig. 1. List of isolated compounds (**1-5**).
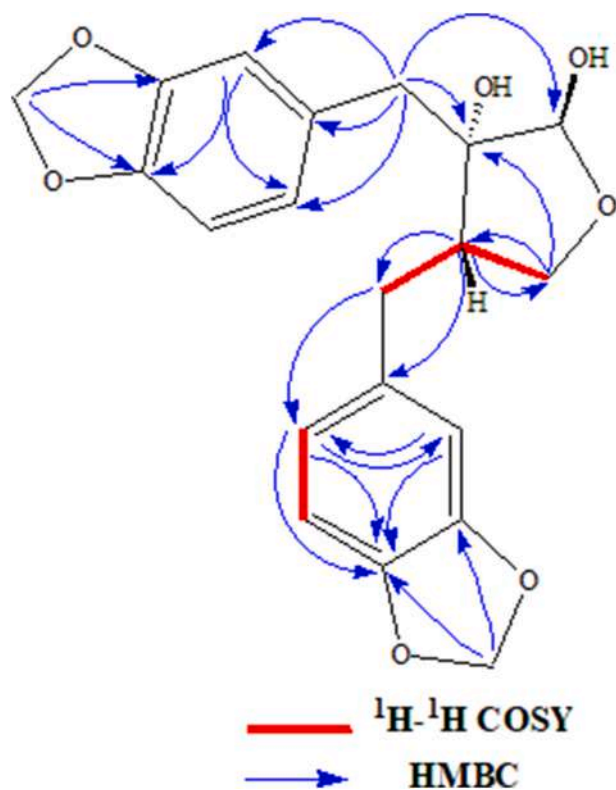
Fig. 2. Key ^{1}H–^{1}H COSY and HMBC correlations in compound **1**.

configuration is correct. Furthermore, the absence of cross peak correlation between H-9 and H-8′ in NOESY spectrum (Fig. S7) confirms the difference in their spatial orientation. Accordingly, **1** was determined as 8α-hydroxy cubebin and trivially named as Glandularin.

Compound **2**, a buff amorphous solid with the molecular formula $C_{58}H_{94}O_{25}$, gave a *quasi*-molecular ion peak at *m/z* 1189.5988 [M-H]⁻ (calcd. for $C_{58}H_{93}O_{25}$, 1189.6006) in its negative mode HRESIMS spectrum, and a sodiated molecular ion peak at *m/z* 1213.6094 [M+Na]⁺ (calcd. for $C_{58}H_{94}O_{25}Na$, 1213.5982) in its positive mode HRESIMS (Fig. S15 and S16). The IR spectrum of compound **2** showed characteristic bands of hydroxyl, ester, and glycosidic C–O at 3409, 2953, 1705, and 1055 cm⁻¹, respectively. The ^{1}H and ^{13}C-NMR spectra displayed signals characteristic for oleanane saponins derivative. The ^{1}H-NMR spectrum (Fig. S9) (Table 2) displayed seven singlet methyl peaks at δ_H 0.88, 1.01, 1.04, 1.12, 1.18, 1.31, 1.83 (each 3H, s), an axial proton attached to a hydroxylated carbon C-3 at δ_H 3.41 (dd, *J* = 9.6, 3.2 Hz), a methine proton attached to C-16 at δ_H 5.31 (br s) and an olefinic proton (H-12) at δ_H 5.65 (br s) indicated that it could be a Δ^{12}-16-hydroxyoleanene derivative. The combined spectral data of the aglycone part of **2** were in agreement with reported data of echinocystic acid (Figs. 1 and 4A) (Nagao et al., 1989; Jæger et al., 2017). The ^{13}C-NMR (Fig. S10) (Table 2) chemical shifts revealed the downfield shifting of C-3 and upfield shifting of C-28 suggesting the presence of two points of glycosidation, one at C-3 (δ_C 89.4) through an ether bridge, and the other esterifying the acid at carbonyl carbon C-28 (δ_C 176.5) of the aglycone. The length of the glycosidic ether-linked chain at position **3** of the aglycone was reduced to a single unit. It was identified as a β-D-glucose with its doublet anomeric proton at δ_H 4.95 (d, *J* = 8.0 Hz), which is correlated to its anomeric carbon (δ_C 107.4) in the HSQC experiment (Fig. S11). Proposition of the usual β-anomeric configuration for this sugar was based on the observation of the anomeric proton's large coupling constant value (*J* = 8.0 Hz). The attachment of the β-D-glucose moiety to C-3 was confirmed by the presence of correlations

between the anomeric proton (δ_H 4.95) with C-3 of the aglycone (δ_C 89.4), and vice versa between H-3 (δ_H 3.41) and the anomeric carbon (δ_C 107.4) in HMBC spectrum (Fig. S12) (Fig. 4B). Further investigation of NMR experiments allowed the detection of proton and carbon resonances of a tetrasaccharide chain composed of the most inner sugar arabinose, xylose, and two rhamnose moieties attached to C-28 (δ_C 176.5). The four anomeric protons for this chain were displayed at δ_H 5.18 (d, *J* = 7.6 Hz), 5.66 (br s), 5.86 (br s), and 6.56 (br s), bounded to carbons at δ_C 105.9, 101.9, 105.0, and 93.7, respectively, in the HSQC spectrum (Fig. S11). Among the four sugars (arabinose, rhamnose, and xylose), the ^{1}H-NMR data revealed that only xylose showed β-anomeric configuration, which was characterized by large trans-diaxial coupling constant value of its anomeric proton (*J* = 7.6 Hz), and the other two (arabinose and rhamnose) possess an α-configuration based on the scale of coupling constant values (all broad singlets) (Ishii et al., 1981; Lee et al., 2002; Jæger et al., 2017). The construction of the tetrasaccharide chain was completed using the cross peak correlations shown in ^{1}H–^{1}H COSY, TOCSY and HMBC spectra (Fig. S12, S13 and S14) (Fig. 4B). In the HMBC spectrum (Fig. S12) (Fig. 4B), H-1 of Xyl (δ_H 5.18) was long-range coupled with C-4 (δ_C 77.9) of Rha-I, H-1 (δ_H 5.85) of Rha-II showed cross peak correlation with C-3 (δ_C 81.6) of Rha-I, also H-1 (δ_H 5.66) of Rha-I displayed correlation with C-2' (δ_C 76.3) of Ara, and H-1 (δ_H 6.56) of Ara was coupled with the carbonyl carbon of the aglycone C-28 (δ_C 176.5), which confirmed the sugar chain at C-28 to be β-D-xylopyranosyl-(1→4)-[α-L-rhamnopyranosyl-(1→3)]-α-L-rhamnopyranosyl-(1→2)-α-L-arabinopyranosyl ester. According to the literature and NMR values of the reported analogues (Su et al., 2001; Lee et al., 2002; Eskander et al., 2005; Murata et al., 2013), **2** was determined as 3-O-β-D-glycopyranosyl-3β,16α-dihydroxyolean-28-oic acid 28-O-β-D-xylopyranosyl-(1→4)-[α-L-rhamnopyranosyl-(1→3)]-α-L-rhamnopyranosyl-(1→2)-α-L-arabinopyranosyl ester. To the best of our knowledge, this is the first report of this compound in nature.

Compound **3**, was obtained as a buff amorphous solid, its molecular formula $C_{63}H_{102}O_{29}$, was deduced from molecular ion peaks *m/z* 1345.6496 [M + Na]⁺ (calcd for $C_{63}H_{102}O_{29}Na$, 1345.6404) in positive mode HRESIMS, and *m/z* 1357.6131 [M+Cl]⁻ (calcd for $C_{63}H_{102}O_{29}Cl$, 1357.6127) in negative mode HRESIMS (Fig. S23 and S24), which was 132 mass unit more than **2**. The IR spectrum of compound **3** showed bands at 3398 (OH), 2910 (C–H), 1699 (C=O), 1051 (glycosidic C–O) cm⁻¹. The inspection of NMR data (Fig. S17-S22) of compound **3** revealed that ^{1}H and ^{13}C- NMR spectra displayed the same pattern of protons and carbons of the aglycone part and sugar chain attached to C-28 as in compound **2** (Table 2), recommending that an additional pentose sugar moiety attached to C-3 sugar chain. The ^{1}H-NMR data (Fig. S17) (Table 2) showed the anomeric proton of this additional sugar resonating at δ_H 5.28 and coupled with δ_C 109.4 in the HSQC spectrum (Fig. S19). In the ^{1}H-^{1}H COSY experiment (Fig. S21) (Fig. 4C), the anomeric proton of the additional sugar moiety at δ_H 5.28 (d, *J* = 2.4 Hz) was observed to be coupled with a vicinal proton at δ_H 3.80, which appears also as a doublet (d, *J* = 2.4 Hz). This sugar was further characterized in the NMR spectra (Fig. S17 and S18) by two oxygenated methylene groups at δ_C 73.9 and 64.1, and an oxygenated quaternary carbon at δ_C 79.3. Analysis of 1D and 2D-NMR data showed that these findings were best arranged as a β-D-apiofuranosyl (Ishii and Yanagisawa, 1998; Farag et al., 2001; Eskander et al., 2005; Zhang et al., 2018). The sequence of the disaccharide sugar chain at C-3 of the aglycone was determined using HMBC spectrum (Fig. S20) (Fig. 4B); the cross peak correlations between H-1 of β-D-apiose (δ_H 5.28) with C-2 of Glu (δ_C 78.2) and H-1 of Glu (δ_H 4.23) with C-3 of aglycone (δ_C 88.7) (Lu and Yeap Foo, 2000). After reviewing literature (Eskander et al., 2005; Ragab et al., 2010; Meng et al., 2021), the complete structure of **3** was assigned as 3-O-(β-D-apiofuranosyl-(1→2)-β-D-glucopyranosyl)-3β,16 α-dihydroxyolean-28-oic acid 28-O-β-D-xylopyranosyl-(1→4)-[α-L-rhamnopyranosyl-(1→3)]-α-L-rhamnopyranosyl-(1→2)-α-L-arabinopyranosyl ester.
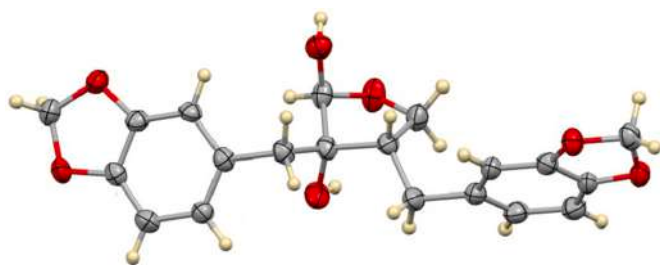
Fig. 3. Stereochemical structure of compound **1**.

The UPLC-UV/MS method was used to characterise the monosaccharides in glycosidic compounds **2** and **3** to confirm their identities and absolute configurations. The hydrolysates of the isolated compounds, together with the monosaccharide's standards, were derivatized to diastereomeric arylthiocarbamates according to the reported procedures (Tanaka et al., 2007). The differentiation between the ᴅ- and ʟ-configurations of each sugar was done by comparing its retention time to that of the standards. Derivatives of ᴅ-glucose (t_R 14.7 min), ᴅ-xylose (t_R 16.2 min), ʟ-rhamnose (t_R 22.4 min), and ʟ-arabinose (t_R 17.4 min) were identified as the sugar moieties of **2** and **3** based on comparisons with derivatives of authentic samples; ᴅ-glucose (t_R 14.7 min), ʟ-glucose (t_R 13.3 min), ᴅ-xylose (t_R 16.2 min), ʟ-xylose (t_R 14.8 min), ʟ-rhamnose (t_R 22.4 min), ᴅ-arabinose (t_R 17.4 min), and ʟ-arabinose (t_R 16.9 min) (Wang et al., 2012). The obtained mass spectra, on the other hand, were typical for pentoses (ᴅ-xylose and ʟ-arabinose), hexoses (ᴅ-glucose) and deoxy hexoses (ʟ-rhamose), showing characteristic ions at *m/z* 403, 433, and 417, respectively (Wang et al., 2012). Therefore, from the obtained chromatograms and mass spectra, in addition to the published NMR data, the sugar moieties of compounds **2** and **3** were identified as

ᴅ-(+)-glucose, ʟ-(−)-rhamnose, ᴅ-(+)-xylose, and ʟ-(−)-arabinose.

Known compounds, **4** and **5** (Fig. 1), were characterized by comparing their spectral data with the NMR data of published analogues. These compounds were identified as adenosine (**4**) (Ciuffreda et al., 2007) and lamiide (**5**) (Güvenalp et al., 2006).

According to our earlier research, the chemotaxonomy of the genus *Glandularia* has been a subject of interest in order to aid in the establishment of the genus' phytochemical profile (Mohamed et al., 2020). We have previously reported the isolation of oleanane based triterpenoidal saponins as chemotaxonomic marker for genus *Glandularia* (Mohamed et al., 2020). In this study, we have also isolated one dibenzylbutyrolactolic lignan together with two echinocystic acid based triterpenoidal saponins, which have been detected for the first time in this genus. Hence, compounds **1–3** could be considered as valuable chemotaxonomic markers for genus *Glandularia* and confirm the unique identity of our plant under investigation.

2.2. Molecular docking

Modelling and docking simulations of the isolated compounds **1** and **2** were performed using Molecular Operating Environment (MOE) software ("Molecular Operating Environment (MOE) 2014.0901," n.d.) and the crystal structure of the murine inducible nitric oxide synthase iNOS; (PDB: 4UX6) (Cheshire et al., 2011).

The accuracy of MOE docking protocol was validated and confirmed by re-docking the co-crystallized ligand inside the active site of iNOS, where the docked ligand showed *S* score of −8.41 kcal/mol with RMSD 1.69 Å (Fig. S25). Also, in order to rationalize the biological results of isolated compounds, the docking study was performed and compared with the positive control; parthenolide (Fig. S26).

On the basis of docking score analysis against the protein target, the saponin structure (**2**) showed higher negative score (−9.59 kcal/mol)
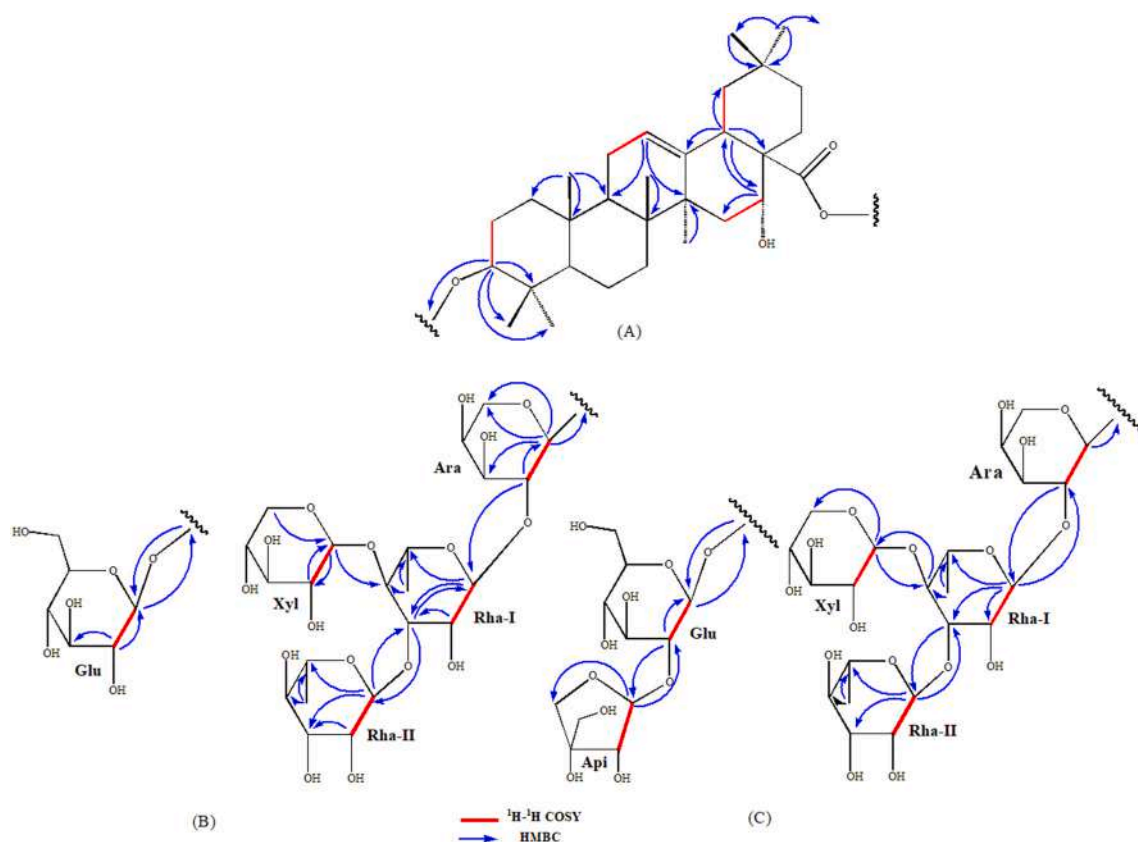

Fig. 4. A) Key ^{1}H–^{1}H COSY and HMBC correlations of aglycone part of **2** and **3**. B) Key ^{1}H–^{1}H COSY and HMBC correlations of C-3 and C-28 sugar chains of **2**. C) Key ^{1}H–^{1}H COSY and HMBC correlations of C-3 and C-28 sugar chains of **3**.

than the lignan one (**1**) (−6.56 kcal/mol) which is compatible with the biological results. Binding mode analysis also revealed that both compounds bind snugly within the larger active-site cavity complexed with heme that coordinates to Cys194. The cavity gate is large enough to allow the diffusion of both compounds where the heme nearly closes the opposite surface. The sugar moiety at C-3 of the triterpenoid saponin structure resides in the main channel of the cavity over the heme structure forming three H-bond interactions with Glu371 (2.75 and 3.35 Å) and Gln 257 (3.03 Å). The sugar chain at the cavity opening stabilizes the complex by forming multiple H-bond interactions with Gln486 (3.01 Å), Glu488 (3.32 Å), Glu279 (3.35 and 3.24 Å), and Asn348 (3.00 Å) (Fig. 5B). Moreover, the hydrophobic aglycone reinforces the binding by forming hydrophobic interaction with Val346, Trp475, Met114, Ala276, and Pro344. Other ligand interactions within the active site include hydrophobic ones with Glu371, Gln257, Tyr485, Asn348, Ser256, Asn115, Gln381, Glu488, Glu279. Interestingly, docking of an assumed product of saponin structure, obtained via expected hydrolysis at the glycosidic ester bond, improved the overall binding profile of the compound. The retained sugar moiety at position C-3 of the hydrolyzed saponin structure accepts an additional H-bond from Tyr341 (3.25 Å), as well as the hydroxyl group at C-16 of the triterpenoid moiety donates a new H-bond to Ala276 (3.29 Å) at the cavity gate (Fig. 5C). On the other hand, the flexibility profile of compound **1** weakens its binding mode within the active site. The tertahydrofuran moiety donates two H-bond interactions to Glu371 (2.78) and Asp376 (3.28) while accepting one H-bond from Gln257 (3.12). However, one of the benzodioxol moieties of compound **1** is located inside the main channel of the cavity and slightly stacks with the heme structure, while the other one fluctuates to the gate (Fig. 5A). Docking results revealed that the dioxol group in the structure of compound **1**, rather than dihydroxy, on both sides of the tetrahydrofuran moiety increases the chance for the compound flexibility and in turn decreasing its probability of forming H-bond interactions deep inside the active site (Fig. S27 and S28).

To conclude, molecular docking study supported the biological data of the isolated compounds and proposed a mechanism for the anti-inflammatory activity of the saponin (compound **2**) via acting as competitive inhibitor for the substrate; L-arginine at its binding site within iNOS.

2.3. Prediction of pharmacokinetic properties (ADMET)

The ADMET properties of compounds **1** and **2** as well as the assumed hydrolysate of compound **2** under docking study were calculated using the pkCSM-pharmacokinetics server (http://biosig.unimelb.edu.au/pkcsm/) by providing SMILES (Simplified Molecule Input Line Entry Specification) of the compounds generated by ChemDraw software. Physicochemical properties of compounds **1** and **2**, together with hydrolysate of compound **2** are listed in Table 3.

The efficacy of any compound as an orally active drug was determined using Caco2 permeability and intestinal absorption models. Only compound **1** which obeys lipiniski's rules of five shows the Caco2 permeability value in positive integer and demonstrates its intestinal absorption ability with 96%, while compound **2** is considered to be very poorly absorbed from the human intestine. However, hydrolysate of compound **2** demonstrates better intestinal absorption by 38%, which considered as reasonable absorption, upon lack of the sugar chain at C-28 of the hydrolyzed saponin structure. Upon reaching the colonic tract, saponins were reported to be hydrolysed mainly via the action of the microbiota (Navarro del Hierro et al., 2018). The next important variable in absorption is skin permeability, and all compounds have permeability values of less than −2.5 log Kp, suggesting poor permeability. P-glycoprotein is a component of the ATP-binding cassette (ABC) transporter, which is required for active molecular transport across cell membranes. Only compound **2** and its predicted hydrolysate were discovered to be P-glycoprotein substrates, suggesting that they can move through the cell membrane via the ABC transporter. Besides this,
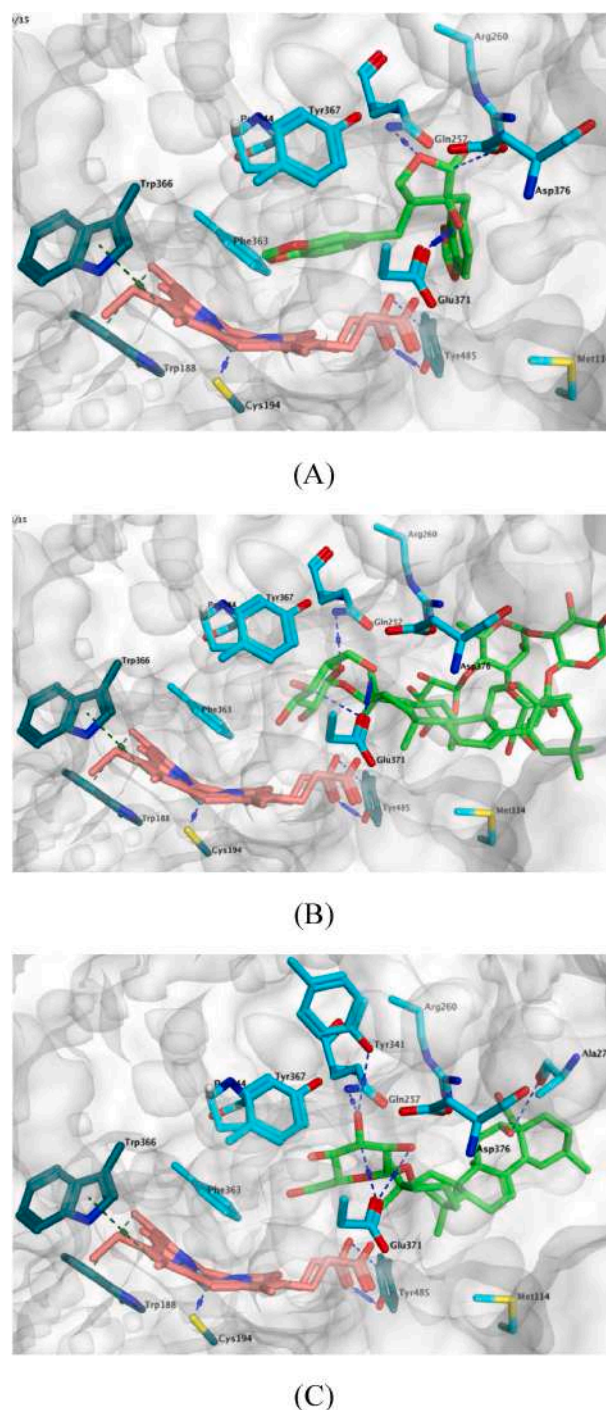

(A)

(B)

(C)

Fig. 5. A) 3D-docked model of compound **1** within the active site of iNOS; heme was shown in dark pink co-ordinating with amino acid residue; Cys194, (shown in dark cyan). B) 3D-docked model of compound **2** within the active site of iNOS; heme was shown in dark pink co-ordinating with amino acid residue; Cys194, (shown in dark cyan). C) 3D-docked model of hydrolysate of compound **2** within the active site of iNOS; heme was shown in dark pink co-ordinating with amino acid residue; Cys194, (shown in dark cyan).

compounds **1** and **2** were found to be effective as inhibitors for P-glycoprotein I transporters and ineffective as inhibitors for P-glycoprotein II transporters. On the other hand, hydrolysate of compound **2** was discovered to be ineffective in both cases, implying that it is unable to inhibit both of these drug efflux pumps. The VDss assay is used to measure the total amount of drug required for uniform drug distribution in the blood. However, both compounds showed low VDss values

Table 3

Physicochemical properties of compounds **1**, **2** and the suggested hydrolysate of compound **2**

Descriptor	Compounds		
	1	2	Hydrolysate of compound 2
Molecular Weight	372.373	1191.365	634.851
LogP	1.6251	−1.9069	4.0286
#Rotatable Bonds	4	11	4
#Acceptors	7	25	8
#Donors	2	14	6
Surface Area	155.547	483.209	267.942

indicating slow diffusion in blood. The permeability of the Blood-Brain Barrier (BBB) determines a compound's ability to move to the brain. They will be poorly distributed to the brain if the logBB values are less than −1. Only compound **1** would be able to cross BBB. However, the blood brain permeability surface area product (logPS) is a more direct and accurate measurement. All compounds with logPS < −3 are considered unable to penetrate the CNS. Predicted metabolism of the compounds in the body was assessed using seven different cytochrome models. Compound **1** is likely to be metabolized by CYP3A4 and also going to be a CYP1A2 and CYP3A4 inhibitor. On the other hand, compound **2** is neither a substrate nor an inhibitor for cytochrome P450.

All compounds had different total clearance rates, and only compound **2** appeared as a substrate for organic cation transporter 2 (OCT2). Furthermore, none of them predicted AMES toxicity, suggesting that these compounds are neither carcinogenic nor mutagenic. Skin sensitisation and hepatotoxicity were not seen in any of the compounds. The toxic effects of compounds are shown in Table 4 along with other ADMET properties.

2.4. Inhibition of iNOS activity

Nitric oxide (NO) is one of the main inflammatory mediators involved in both inflammation and angiogenesis processes. The production of NO depends on cytokine-induced expression of inducible nitric oxide synthase (iNOS) (Cassini-Vieira et al., 2015). It is produced *in vivo* from the natural substrate; L-arginene and oxygen by either endothelial (eNOS), neuronal (nNOS) and inducible nitric oxide synthase (iNOS) (Fischmann et al., 1999; Subedi et al., 2021). During rheumatoid arthritis and asthma, cytokines induce prolonged and over-production of NO merely by iNOS which may result in increased cytotoxicity (Cheshire et al., 2011). Hence, iNOS is a primary mediator of inflammation and many drugs nowadays are targeting inhibition of iNOS to reduce inflammation process and adverse effects associated with it (Green et al., 1994). Some naturally occurring saponins and lignans were found to down-regulate NO production induced by inflammatory mediators (Navarro et al., 2018; He et al., 2019). Compounds **1–3** were tested for their anti-inflammatory activity through the inhibition of iNOS mediator. Compound **1** exhibited moderate inhibition activity on iNOS with IC_{50} value of 49.7 µM, while compound **2** showed relatively significant activity with IC_{50} value of 6.6 µM. The obtained results were compared to parthenolide, the postive control, which showed IC_{50} value of 1.2 µM. All results are listed in Table 5.

Table 5

Inhibition of iNOS activity of the isolated compounds **1–3**.

Compound no.	Inhibition of iNOS	% cell death at 25 µg/mL
	IC_{50} µM (µg/mL)	
1	49.7 (18.5)	62
2	6.6 (7.9)	86
3	[a]NA	[a]NA
[b]Parthenolide	1.2 (0.29)	94

[a] NA, not active.
[b] Positive control.

Table 4

ADMET properties of compounds **1**, **2** and the suggested hydrolysate of compound **2**

Property	Model Name	Predicted Values of compounds			Unit
		1	2	Hydrolyste of compound 2	
Absorption	Water solubility	−3.347	−2.886	−3.363	Numeric (log mol/L)
	Caco2 permeability	1.199	−0.754	−0.331	Numeric (log Papp in 10 cm/s)
	Intestinal absorption (human)	96.372	1.871	38.181	Numeric (% Absorbed)
	Skin Permeability	−2.752	−2.735	−2.735	Numeric (log Kp)
	P-glycoprotein substrate	No	Yes	Yes	Categorical (Yes/No)
	P-glycoprotein I inhibitor	Yes	Yes	No	Categorical (Yes/No)
	P-glycoprotein II inhibitor	No	No	No	Categorical (Yes/No)
Distribution	VDss (human)	−0.164	−0.194	−0.968	Numeric (log L/kg)
	Fraction unbound (human)	0.048	0.378	0.182	Numeric (Fu)
	BBB permeability	−0.658	−3.453	−1.64	Numeric (log BB)
	CNS permeability	−3.36	−5.464	−2.876	Numeric (log PS)
Metabolism	CYP2D6 substrate	No	No	No	Categorical (Yes/No)
	CYP3A4 substrate	Yes	No	Yes	Categorical (Yes/No)
	CYP1A2 inhibitor	Yes	No	No	Categorical (Yes/No)
	CYP2C19 inhibitor	Yes	No	No	Categorical (Yes/No)
	CYP2C9 inhibitor	No	No	No	Categorical (Yes/No)
	CYP2D6 inhibitor	No	No	No	Categorical (Yes/No)
	CYP3A4 inhibitor	Yes	No	No	Categorical (Yes/No)
Excretion	Total Clearance	0.046	−0.111	−0.003	Numeric (log ml/min/kg)
	Renal OCT2 substrate	No	Yes	No	Categorical (Yes/No)
Toxicity	AMES toxicity	No	No	No	Categorical (Yes/No)
	Max. tolerated dose (human)	−0.217	0.14	−0.466	Numeric (log mg/kg/day)
	hERG I inhibitor	No	No	No	Categorical (Yes/No)
	hERG II inhibitor	No	Yes	No	Categorical (Yes/No)
	Oral Rat Acute Toxicity (LD50)	2.494	2.482	2.75	Numeric (mol/kg)
	Oral Rat Chronic Toxicity (LOAEL)	1.611	8.228	4.482	Numeric (log mg/kg_bw/day)
	Hepatotoxicity	No	No	No	Categorical (Yes/No)
	Skin Sensitisation	No	No	No	Categorical (Yes/No)
	T.Pyriformis toxicity	0.305	0.285	0.285	Numeric (log ug/L)
	Minnow toxicity	−0.054	17.28	3.583	Numeric (log mM)

2.5. Cytotoxic activity of isolated compounds

The cytotoxic activity of compounds **1–3** was investigated using an *in vitro* assay against a series of human solid tumor cells including SK-MEL (malignant melanoma), KB (oral epidermal carcinoma), BT-549 (breast ductal carcinoma), SK-OV-3 (ovary carcinoma), and LLC-PK1 (renal epithelial cells). Their cytotoxicity was also determined against noncancerous mammalian VERO cells (renal fibroblast) for comparison. The cytotoxic potencies of these compounds are expressed in terms of IC_{50} values, as shown in Table 6. Compound **1** showed moderate cytotoxic activity against SK-MEL with IC_{50} value of 45.6 μM, in addition to cytotoxic activity against VERO cells with IC_{50} value of 37.6 μM, indicating the un-selectivity to tumor cells. To the best of our knowledge, cubebin (**1a**), and its synthetic derivatives with varying functional moieties, showed significant anticancer activity upon testing against six human cancer cell lines (A549, K562, SiHa, KB, HCT116 and HT29) using MTT assay (Rajalekshmi et al., 2016). Compound **2** showed relatively potent cytotoxic activity against all the tested cell lines with IC_{50} values ranging between <5.3 and 10.1 μM. Compound **3** showed moderate cytotoxic activity against KB, BT-549, SK-OV-3, and renal epithelial cells with IC_{50} values ranging between 8.3 and 18.9 μM. All the results were compared to doxorubicin which was used as positive control with IC_{50} values ranging between 2.6 and 9.2 μM.

3. Conclusions

Three previously undescribed compounds (**1–3**) and two known compounds (**4–5**) were isolated from the leaves of *G. hybrida.* Their structures were determined by NMR and HRESIMS data analysis. Additionally, *in silico* and *in vitro* assessments of some biological activities for compounds **1–3** revealed that these compounds could be considered as promising cytotoxic agents and inhibitors of iNOS mediator .

4. Experimental section

4.1. General experimental procedures

Optical rotations were recorded at room temperature using a Rudolph AutoPol IV automatic polarimeter (Rudolph Research Analytical, Hackettstown, NJ, USA); UV spectra were recorded by a Hewlett-Packard 8452 A UV–Vis spectrometer (American Laboratory Trading, CT, USA); IR spectra were acquired using Bruker Tensor 27 and MIRacle ATR FT−IR spectrometers (Bruker Scientific Instruments, Bruker Optics, MA, USA); 1D and 2D NMR spectra were recorded in DMSO-d_6 or pyridine-d_5 and acquired on Bruker Avance DRX spectrometer at 400 MHz (^{1}H) and 100 MHz (^{13}C), 600 MHz (^{1}H) and 150 MHz (^{13}C). The chemical shifts are given in δ (ppm) and were calibrated using the residual solvent signals; coupling constants (J) are reported in Hertz (Hz). The signals in the spectra are described as s (singlet), d (doublet), t (triplet), m (multiplet) and br (broad resonances). High-resolution mass spectra were recorded using a HRESI-TOFMS spectrometer (Agilent Series 1100 SL, ESI source model #G1969A, Agilent Technologies, Palo Alto, CA, USA). Solvents used for extraction and isolation purposes were analytical grade (Fisher Scientific, Fair Lawn, NJ, USA). Column chromatography was carried out using silica gel 60 F_{254} (40–65 μm, Merck, Darmstadt, Germany), Sephadex LH-20 (0.25–0.1 mm, Mitsubishi Kagaku, Tokyo, Japan), and reversed-phase C_{18} silica gel (Polarbond, JT Baker). TLC was performed on silica 60 F_{254} (0.2 mm, Merck, Darmstadt, Germany) pre-coated aluminum sheets. Visualization of spots was done by spraying with 5% vanillin (Sigma-Aldrich) solution in conc. H_2SO_4–EtOH (5:95) followed by heating.

4.2. Plant material

During the flowering stage, the fresh leaves of *G. × hybrida* (Groenl. & Rümpler) G.L. Nesom & Pruski (unresolved name: see The Plant List http://www.theplantlist. org) (Verbenaceae) were collected on April–May 2013 from Hebat El Nile nurseries, El-Manial, Cairo, Egypt, at geographical coordinates 30° 01′ 08″ N 31° 13′ 02″ E and an altitude of 20 m. The identity of the selected species was authenticated by (the late) Prof. N. E. Keltawy, Professor of Ornamental Horticulture and Floriculture, Faculty of Agriculture, Assiut University, Assiut, Egypt. A voucher specimen number GHV-2013 was recorded and lodged at the Herbarium of Pharmacognosy Department, Faculty of Pharmacy, Assiut University, Assiut, Egypt.

4.3. Extraction and isolation

The air dried leaves (4 kg) were ground and extracted at room temperature in 70% (v/v) aqueous ethanol (4 × 6 L). The obtained extract was decanted, filtered, and combined extracts were concentrated using rotary evaporator with a water bath of 40 °C, to get a concentrated extract (284 g). The obtained extract was suspended in distilled water (250 mL) and defatted by liquid-liquid partition using *n*-hexane solvent. The remaining aqueous extract was collected and concentrated under reduced pressure to get defatted residue (170 g). About 70 g of the defatted extract was fractionated on vacuum liquid chromatography (VLC) using C-18-reversed phase silica gel (80 × 7.0 cm, 500 g) as stationary phase, and by increasing MeOH in MeOH–H_2O system (1 L 0%, 1.5 L 20%, 2 L 40%, 2 L 60%, 2 L 80% and 2 L 100%) with the collection of 300 mL fractions. The fractions were collected based on their TLC profile resulting in six main fractions (GH-I:GH-VI). TLC analysis of obtained fractions recommended the presence of promising compounds in fractions GH-II (5.3 g), GH-III (7.1 g) and GH-V (6.3 g). About 1 g of fraction GH-II was subjected to column chromatography (CC) using sephadex LH-20 as stationary phase (150 × 2.3 cm, 150 g) and MeOH as eluent (500 mL) to yield compounds **5** (5.3 mg) and **4** (7.6 mg), respectively. A part of fraction GH-III (1 g) was further separated on sephadex LH-20 CC (150 × 2.3 cm, 150 g), using MeOH (500 mL) as eluent to get three subfractions GH–III–1 to GH–III–3. Subfraction GH–III–1 (253 mg) was further purified on silica gel CC, using system EtOAc-CH_2Cl_2–MeOH–H_2O with gradient elution program [10:6:5:1.25 & 6:4:5:1.25, (250 mL)] to afford compounds **2** (15.4 mg) and **3 (**10.8 mg**)**, respectively. About 1.7 g of fraction GH-V was subjected to silica gel CC (100 × 1.5 cm, 80 g) using CH_2Cl_2–MeOH [95:5, (500 mL)], to get subfraction GH-V-1 (273 mg), which was further purified on silica gel CC (80 × 1 cm, 25 g) using EtOAc-CH_2Cl_2–MeOH–H_2O as eluent in isocratic elution manner [17:10:4:1, (250 mL)] to isolate compound **1** (7.3 mg).

4.4. Determination of absolute configuration of sugar

The determination of the composition of sugar moieties and their configuration was performed according to UPLC-UV/MS method (Wang et al., 2012). Compounds **2** and **3** were acid hydrolyzed by dissolving

Table 6
Cytotoxicity of the isolated compounds **1**–3.

Compounds	IC_{50} μM ([a]μg/mL)					
	SK-MEL	KB	BT-549	SK-OV-3	LLC-PK1	VERO
1	45.6 (17)	[b]NA	[b]NA	[b]NA	[b]NA	37.6 (14)
2	<5.3 (<6.25)	9.2 (11)	10.1 (12)	10.1 (12)	8.4 (10)	<5.3 (<6.25)
3	[b]NA	13.5 (18)	15.0 (20)	8.3 (11)	18.9 (25)	[b]NA
[c]**Doxorubicin**	2.8 (1.5)	2.9 (1.6)	3.1 (1.7)	2.6 (1.4)	2.6 (1.4)	9.2 (5)

[a] The highest concentration tested was 25 μg/mL.

[b] NA, not active.

[c] Positive control

about 1 mg of each compound in 1 mL of 2N HCl. The dissolved samples were heated in a water bath to 95 °C for 1 h. After hydrolysis, the reaction mixture was chilled, treated with liquid ammonia, and completely dried with N_2 gas. Monosaccharide standards together with the hydrolysates of **2** and **3** were derivatized (Tanaka et al., 2007; Wang et al., 2012). The final derivatives were analysed by UPLCTM BEH C-18 column (100 mm × 2.1 mm), with particle size 1.7 μM; mobile phase, 0.05% formic acid in water (A) and acetonitrile/methanol/isopropanol (50:25:25, v/v/v) with 0.05% formic acid (B), flow rate of the mobile phase was set at 0.3 mL/min; PDA detector, UV at 254 nm. The column temperature were maintained at 35 °C. The experiment was carried out in gradient elution manner: starting with system 14% B to 16.5% B in 22 min, and then increasing B to 100% in the subsequent 0.5 min. The ESI source of single quadrpole mass spectrometer (SQD) was adjusted to positive mode. The configurations of the sugar units were determined through comparing retention times and mass spectra with that of the used reference standards (Wang et al., 2012). The standard monosaccharides included: D-(+)-glucose, L-(−)-glucose, L-(−)-rhamnose, D-(+)-xylose, L-(−)-xylose, L-(−)-arabinose and D-(+)-arabinose.

4.5. X-ray experimental

Intensity data were collected at 90 K to $\theta_{max} = 69.2°$ on a Bruker Kappa Apex-II diffractometer with CuKα radiation. Absorption corrections were done by the multi-scan method. Refinement was done by SHELXL-2018. Hydrogen atoms were visible in difference maps, and were placed in idealized positions, except for those on O, for which positions were refined. The Flack parameter 0.14 (18) is in agreement with the absolute configuration of (−)cubebin. Crystal Data: monoclinic space group P2₁, a = 11.5470 (4), b = 5.5768 (2), c = 13.4963 (5) Å, β = 100.029 (3)°, 13,377 reflections collected, 3180 unique, 2677 with I > 2σ(I), R = 0.049 for 250 parameters, CCDC 2057610.

4.6. Spectroscopic data of compounds (1–3)

4.6.1. Glandularin (1)

Colourless residue; $[\alpha]^{20}_D$−19 (*c* 0.1, MeOH); UV (MeOH) λ_{max} 281 and 228 nm; ^1H and ^{13}C-NMR data (DMSO-d_6, 400/100 MHz), see Table 1; HRESIMS *m/z* 371.1176 [M-H]⁻ (calcd. for $C_{20}H_{19}O_7$, 371.1131), *m/z* 417.1219 [M + HCOO]⁻ (calcd. for $C_{21}H_{21}O_9$ 417.1191) negative mode.

4.6.2. 3-O-β-D-glycopyranosyl-3β,16α-dihydroxyolean-28-oic acid 28-O-β-D-xylopyranosyl-(1→4)-[α-L-rhamnopyranosyl-(1 →3)]-α-L-rhamnopyranosyl-(1→2)-α-L-arabinopyranosyl ester (2)

Buff amorphous solid; $[\alpha]^{20}_D$−120 (*c* 0.1, MeOH); IR (KBr) ν_{max} 3409, 2953, 1705, 1683, 1370, 1055 cm⁻1; UV (MeOH) λ_{max} 202 nm; ^1H and ^{13}C-NMR data (Pyridine-d_5, 400/100 MHz), see Table 2; HRESIMS *m/z* 1189.5988 [M-H]⁻ (calcd. for $C_{58}H_{93}O_{25}$, 1189.6006) negative mode, *m/z* 1213.6094 [M+Na]⁺ (calcd. for $C_{58}H_{94}O_{25}Na$, 1213.5982) positive mode.

4.6.3. 3-O-(β-D-apiofuranosyl-(1→2)-β-D-glucopyranosyl)-3β,16α-dihydroxyolean-28-oic acid 28-O-β-D-xylopyranosyl-(1→4)-[α-L-rhamnopyranosyl-(1→3)]-α-L-rhamnopyranosyl-(1→2)-α-L-arabinopyranosyl ester (3)

Buff amorphous solid; $[\alpha]^{20}_D$−100 (*c* 0.1, MeOH); IR (KBr) ν_{max} 3398, 2910, 1699, 1630, 1373, 1051 cm⁻¹; UV (MeOH) λ_{max} 203 nm; ^1H and ^{13}C-NMR data (DMSO-d_6, 600/150 MHz), see Table 2; HRESIMS *m/z* 1345.6496 [M+Na]⁺ (calcd for $C_{63}H_{102}O_{29}Na$, 1345.6404) positive mode, *m/z* 1357.6131 [M+Cl]⁻ (calcd for $C_{63}H_{102}O_{29}Cl$, 1357.6127) negative mode.

4.7. Molecular docking

The molecular modelling calculations and docking simulation

studies were performed on a Processor Intel(R) Pentium(R) CPU N3510@ 1.99 GHz and 4 GB Memory with Microsoft Windows 8.1 pro (64 Bit) operating system using Molecular Operating Environment (MOE 2019.0102, 2020; Chemical Computing Group, Canada) as the computational software. All MOE minimizations were performed until a RMSD gradient of 0.01 kcal/mol/Å with the force field (MMFF94x) to calculate the partial charges automatically using Gas phase solvation. Before simulations, the protein was protonated using LigX function and the monomer was isolated. Triangle matching with London dG scoring was chosen for initial placement, and then the top 30 poses were refined using force field (MMFF94x) and GBVI/WSA dG scoring. The output database dock file was created with different poses for each ligand and arranged according to the final score function (*S*), which is the score of the last stage that was not set to zero.

4.8. Biological activity evaluations

4.8.1. Assay for the inhibition of iNOS activity

Mouse macrophages (RAW264.7) were used in this assay, which were grown in RPMI media supplemented with 10% bovine calf serum, 100 g/mL streptomycin, and 100 U/mL penicillin G sodium. Cells were implanted in 96-well plates (100,000 cells/well) and incubated for 24 h until they reach 75% or higher confluence.

The cells were exposed to the test compounds (**1–3**), then after 30 min, LPS (Sigma-Aldrich) (5 μg/mL) was added and cells were further incubated for 24 h. The concentration of NO was done by estimation of the level of nitrite in the supernatant of the cell culture using Griess reagent (Sigma-Aldrich). This was considered as an indication for the iNOS activity. Inhibition of iNOS activity achieved by the test compound was calculated in comparison to the negative control. Dose-response curves were used to determine the IC_{50} values. Parthenolide was included as drug control. (Zhao et al., 2014; Zulfiqar et al., 2017).

4.8.2. Assay for cytotoxic activity

The cytotoxic activity of the isolated compounds (**1–3**) was determined by a cell proliferation assay against a panel of human cancer cell lines (SK-MEL, KB, BT-549, SK-OV-3, LLC-PK1), as well as VERO cell line (renal fibroblast). Cell lines have been obtained from the American Type Culture Collection (ATCC, Rockville, MD, USA). The cells were seeded in 96-well plates at a density of 10,000 cells/well and incubated for 24 h. Test samples at various dilutions were added and the cells were further incubated for 48 h. The cell viability was determined by using a tetrazolium dye (WST-8) which is converted to a water soluble formazan product in the presence of 1-methoxy PMS by the activity of cellular dehydrogenases. The amount of resulting formazan was measured by reading the absorbance at λ = 450 nm which is directly proportional to the number of viable cells. The viability of sample treated cells was calculated in comparison to the vehicle treated cells and the concentration responsible for decreasing 50% cell viability (IC_{50} value) was calculated from the concentration response curves. Doxorubicin was included as the positive control for cytotoxicity assay (Zulfiqar et al., 2017).

Declaration of competing interest

The authors declare that they have no known competing financial interests or personal relationships that could have appeared to influence the work reported in this paper.

Appendix A. Supplementary data

Supplementary data to this article can be found online at https://doi.org/10.1016/j.phytochem.2021.113054.

References

Ahmed, M.A.M., Mohamed, N.M., Woodman, T.J., Kociok-Köhn, G., Blagbrough, I.S., 2021. Loganin-type iridoids as chemotaxonomic markers in *Glandularia gooddingii* (Briq.) Solbrig. Phytochem. Lett. 44, 68–73. https://doi.org/10.1016/j.phytol.2021.04.003.

Cassini-Vieira, P., Araújo, F.A., Da Costa Dias, F.L., Russo, R.C., Andrade, S.P., Teixeira, M.M., Barcelos, L.S., 2015. iNOS activity modulates inflammation, angiogenesis, and tissue fibrosis in polyether-polyurethane synthetic implants. Mediat. Inflamm. https://doi.org/10.1155/2015/138461, 2015.

Cheshire, D.R., Åberg, A., Andersson, G.M.K., Andrews, G., Beaton, H.G., Birkinshaw, T. N., Boughton-Smith, N., Connolly, S., Cook, T.R., Cooper, A., Cooper, S.L., Cox, D., Dixon, J., Gensmantel, N., Hamley, P.J., Harrison, R., Hartopp, P., Käck, H., Leeson, P.D., Luker, T., Mete, A., Millichip, I., Nicholls, D.J., Pimm, A.D., St-Gallay, S.A., Wallace, A.V., 2011. The discovery of novel, potent and highly selective inhibitors of inducible nitric oxide synthase (iNOS). Bioorg. Med. Chem. Lett 21, 2468–2471. https://doi.org/10.1016/j.bmcl.2011.02.061.

Ciuffreda, P., Casati, S., Manzocchi, A., 2007. Complete ^{1}H and ^{13}C-NMR spectral assignment of alpha- and beta-adenosine, 2'-deoxyadenosine and their acetate derivatives. Magn. Reson. Chem. 45, 781–784. https://doi.org/10.1002/mrc.

Eskander, J., Lavaud, C., Abdel-khalik, S.M., Soliman, H.S.M., Mahmoud, I.I., Long, C., 2005. Saponins from the leaves of *Mimusops laurifolia*. J. Nat. Prod. 68, 832–841. https://doi.org/10.1021/np049582e.

Farag, S.F., Ahmed, A.S., Terashima, K., Takaya, Y., Niwa, M., 2001. Isoflavonoid glycosides from *Dalbergia sissoo*. Phytochemistry 57, 1263–1268. https://doi.org/10.1016/S0031-9422(01)00195-9.

Fischmann, T.O., Hruza, A., Niu, X. Da, Fossetta, J.D., Lunn, C.A., Dolphin, E., Prongay, A.J., Reichert, P., Lundell, D.J., Narula, S.K., Weber, P.C., 1999. Structural characterization of nitric oxide synthase isoforms reveals striking active-site conservation. Nat. Struct. Biol. 6, 233–242. https://doi.org/10.1038/6675.

Green, S.J., Scheller, L.F., Marletta, M.A., Seguin, M.C., Klotz, F.W., Slayter, M., Nelson, B.J., Nacy, C.A., 1994. Nitric oxide: cytokine-regulation of nitric oxide in host resistance to intracellular pathogens. Immunol. Lett. 43, 87–94. https://doi.org/10.1016/0165-2478(94)00158-8.

Güvenalp, Z., Özbek, H., Ünsalar, T., Kazaz, C., Demirezer, L.Ö., 2006. Iridoid, flavonoid, and phenylethanoid glycosides from *Wiedemannia orientalis*. Turk. J. Chem. 30, 391–400.

He, Y., Hu, Z., Li, A., Zhu, Z., Yang, N., Ying, Z., He, J., Wang, C., Yin, S., Cheng, S., 2019. Recent advances in biotransformation of saponins. Molecules 24, 2365. https://doi.org/10.3390/molecules24132365.

Hooft, R.W.W., Straver, L.H., Spek, A.L., 2008. Determination of absolute structure using Bayesian statistics on Bijvoet differences. J. Appl. Crystallogr. 41, 96–103. https://doi.org/10.1107/S0021889807059870.

Ishii, H., Kitagawa, I., Matsushita, K., Shirakawa, K., Tori, K., 1981. The configuration and conformation of the arabinose moiety in Platycodins, saponins isolated from *Platycodon grandiflorum*, and MI-saponins from *Mahuca longifolia* based on ^{13}C- and ^{1}H-NMR spectroscopic evidence: the total structures of the sa. Tetrahedron Lett. 22, 1529–1532.

Ishii, T., Yanagisawa, M., 1998. Synthesis, separation and NMR spectral analysis of methyl apiofuranosides. Carbohydr. Res. 313, 189–192. https://doi.org/10.1016/S0008-6215(98)00262-6.

Jæger, D., Ndi, C.P., Crocoll, C., Simpson, B.S., Khakimov, B., Guzman-Genuino, R.M., Hayball, J.D., Xing, X., Bulone, V., Weinstein, P., Møller, B.L., Semple, S.J., 2017. Isolation and structural characterization of echinocystic acid triterpenoid saponins from the Australian medicinal and food plant *Acacia ligulata*. J. Nat. Prod. 80, 2692–2698. https://doi.org/10.1021/acs.jnatprod.7b00437.

Lee, K.T., Choi, J., Jung, W.T., Nam, J.H., Jung, H.J., Park, H.J., 2002. Structure of a new echinocystic acid bisdesmoside isolated from *Codonopsis lanceolata* roots and the cytotoxic activity of prosapogenins. J. Agric. Food Chem. 50, 4190–4193. https://doi.org/10.1021/jf011647l.

Lu, Y., Yeap Foo, L., 2000. Flavonoid and phenolic glycosides from *Salvia officinalis*. Phytochemistry 55, 263–267. https://doi.org/10.1016/S0031-9422(00)00309-5.

Mabberley, D.J., 2017. Mabberley's Plant-Book, Mabberley's Plant-Book. Cambridge University Press. https://doi.org/10.1017/9781316335581.

Macedo, A.L., Martorano, L.H., de Albuquerque, A.C.F., Fiorot, R.G., Carneiro, J.W.M., Campos, V.R., Vasconcelos, T.R.A., Valverde, A.L., Moreira, D.L., dos Santos, F.M., 2020. Absolute configuration of (−)-cubebin, a classical lignan with pharmacological potential, defined by means of chiroptical spectroscopy. J. Braz. Chem. Soc. 31, 2030–2037. https://doi.org/10.21577/0103-5053.20200103.

Meng, Y., Feng, Z.M., Jiang, J.S., Zhang, X., Zhang, P.C., Yang, Y.N., 2021. Three new monocyclic monoterpenoid *O*-glycosides from the roots of *Glycyrrhiza uralensis*. J. Asian Nat. Prod. Res. 23, 318–324. https://doi.org/10.1080/10286020.2020.1845162.

Mohamed, N.M., Makboul, M.A., Farag, S.F., Wang, Y.H., Mohamed, S.M., Ross, S.A., 2020. Chemosystematically valuable triterpenoid saponins from *Glandularia hybrida*. Phytochemistry 175, 112367. https://doi.org/10.1016/j.phytochem.2020.112367.

Molecular Operating Environment, 2014. 0901, n.d (MOE).

Murata, T., Suzuki, A., Mafune, N., Sato, E., Miyase, T., Yoshizaki, F., 2013. Triterpene saponins from *Clethra barbinervis* and their hyaluronidase inhibitory activities. Chem. Pharm. Bull. 61, 134–143. https://doi.org/10.1248/cpb.c12-00566.

Nagao, T., Hachiyama, S., Okabe, H., Yamauchi, T., 1989. Studies on the constituents of *Aster tataricus* L.f.II. Structures of aster saponins isolated from the root. Chem. Pharm. Bull. 37, 1977. https://doi.org/10.1248/cpb.37.1977, 1983.

Navarro del Hierro, J., Herrera, T., Fornari, T., Reglero, G., Martin, D., 2018. The gastrointestinal behavior of saponins and its significance for their bioavailability and bioactivities. J. Funct. Foods 40, 484–497. https://doi.org/10.1016/J.JFF.2017.11.032.

O'Leary, N., Thode, V., 2016. The genus *Glandularia* (verbenaceae) in Brazil. Ann. Mo. Bot. Gard. 101, 699–749. https://doi.org/10.3417/2014008.

Parsons, S., Flack, H.D., Wagner, T., 2013. Use of intensity quotients and differences in absolute structure refinement. Acta Crystallogr. Sect. B Struct. Sci. Cryst. Eng. Mater. 69, 249–259. https://doi.org/10.1107/S2052519213010014.

Pruski, J.F., Nesom, G.L., 1992. *Glandularia hybrida* (Verbenaceae), a new combination for a common horticultural plant. Brittonia 44, 494–496. https://doi.org/10.2307/2807200.

Ragab, E.A., Hosny, M., Kadry, H.A., Ammar, H.A., 2010. Acylated triterpenoidal saponins and cytokinins from *Gleditsia aquatica*. J. Pharmacogn. Phyther. 2, 24–33.

Rajalekshmi, D.S., Kabeer, F.A., Madhusoodhanan, A.K., Bahulayan, A.K., Prathapan, R., Prakasan, N., Varughese, S., Nair, M.S., 2016. Anticancer activity studies of cubebin isolated from *Piper cubeba* and its synthetic derivatives. Bioorg. Med. Chem. Lett 26, 1767–1771. https://doi.org/10.1016/j.bmcl.2016.02.041.

Su, Y., Koike, K., Guo, D., Satou, T., Liu, J., Zheng, J., Nikaido, T., 2001. New apiose-containing triterpenoid saponins from *Conyza blinii*. Tetrahedron 57, 6721–6726. https://doi.org/10.1016/S0040-4020(01)00632-9.

Subedi, L., Gaire, B.P., Kim, S., Parveen, A., 2021. Nitric oxide as a target for phytochemicals in anti-neuroinflammatory prevention therapy. Int. J. Mol. Sci. 22, 4771. https://doi.org/10.3390/ijms22094771.

Tanaka, T., Nakashima, T., Ueda, T., Tomii, K., Kouno, I., 2007. Facile discrimination of aldose enantiomers by reversed-phase HPLC. Chem. Pharm. Bull. 55, 899–901. https://doi.org/10.1248/cpb.55.899.

Vestena, A., Comerlato, L., Bridi, H., Guerini, L., Vidal Ccana-Ccapatinta, G., Vignoli-Silva, M., Apel, M.A., Fernandes, S., Castro-Gamboa, I., Silveira Zuanazzi, J.A., von Poser, G.L., 2019. Chrysoeriol derivatives and other constituents from *Glandularia selloi*. Phytochem. Lett. 29, 30–34. https://doi.org/10.1016/j.phytol.2018.11.003.

Vidigal, M.C.S., Cavalheiro, A.J., Kato, M.J., Yoshida, M., 1995. Lignans from kernels of *Virola michelii* heckel. Phytochemistry 40, 1259–1261. https://doi.org/10.1016/0031-9422(95)00464-I.

Wang, Y.H., Avula, B., Fu, X., Wang, M., Khan, I.A., 2012. Simultaneous determination of the absolute configuration of twelve monosaccharide enantiomers from natural products in a single injection by a UPLC-UV/MS method. Planta Med. 78, 834–837. https://doi.org/10.1055/s-0031-1298432.

Yuan, Y.W., Olmstead, R.G., 2008. A species-level phylogenetic study of the Verbena complex (Verbenaceae) indicates two independent intergeneric chloroplast transfers. Mol. Phylogenet. Evol. 48, 23–33. https://doi.org/10.1016/j.ympev.2008.04.004.

Zhang, N., Huang, W., Xia, G., Oppong, M.B., Ding, L., Li, P., Qiu, F., 2018. Methods for determination of absolute configuration of monosaccharides. Chinese Herb. Med. 10, 14–22. https://doi.org/10.1016/j.chmed.2017.12.009.

Zhao, J., Khan, S.I., Wang, M., Vasquez, Y., Yang, M.H., Avula, B., Wang, Y.H., Avonto, C., Smillie, T.J., Khan, I.A., 2014. Octulosonic acid derivatives from Roman chamomile (*Chamaemelum nobile*) with activities against inflammation and metabolic disorder. J. Nat. Prod. 77, 509–515. https://doi.org/10.1021/np400780n.

Zulfiqar, F., Khan, S.I., Ross, S.A., Ali, Z., Khan, I.A., 2017. Prenylated flavonol glycosides from *Epimedium grandiflorum*: cytotoxicity and evaluation against inflammation and metabolic disorder. Phytochem. Lett. 20, 160–167. https://doi.org/10.1016/j.phytol.2017.04.027.